Kovove Mater. 60 2022 403–409
DOI: 10.31577/km.2022.6.403

Optimizing microstructure and mechanical properties of NiAl-9Mo alloy by Zr addition and suction casting process

Yongcun Li[1], Wenjun Zhu[1], Yihui Qi[2]*, Yong Wang[1]**

[1]*School of Mechanical Science and Engineering, Northeast Petroleum University, Daqing 163318, P. R. China,*
[2]*School of Materials Science and Engineering, Liaoning University of Technology, Jinzhou 121001, P. R. China*

Received 17 September 2022, received in revised form 30 September 2022, accepted 17 October 2022

Abstract

In the present work, NiAl-9Mo alloys with different addition of Zr were prepared by water--cooled copper mold and suction casting, respectively, and the influence on the microstructure and properties of the alloys was discussed. The results show that the microstructure of the as-cast NiAl-9Mo-xZr (x = 0.5, 1.0, 1.5) alloys is a typical eutectic cell structure, with Ni_2AlZr (Heusler) phases discontinuously distributed in the cell boundaries. The eutectic cells of NiAl--9Mo-1Zr alloy prepared by the suction casting process are refined, and the average eutectic lamella thickness is about 3 μm. The microhardness of the suction-cast NiAl-9Mo-1Zr alloy is 630.0 HV, which is higher than that of the as-cast alloy (396 HV). The high-temperature compressive strength of the as-cast NiAl-9Mo-1Zr alloy is higher than that of the as-cast alloy, which reaches 350 MPa at 1273 K, due to the joint action of fine grain strengthening and the second phase strengthening of the Heusler phase.

K e y w o r d s: NiAl alloy, suction casting, microstructure, grain refinement, high-temperature strength

1. Introduction

The requirement for materials with high-temperature performance is increasing due to the world's fast development in aerospace, energy, and other sectors, particularly in the crucial area of aerospace engines [1–4]. The NiAl alloys with a B2 structure that features a high melting point, low density, high elastic modulus, and outstanding high-temperature oxidation resistance, are the most typical of high--temperature structural materials. However, its applicability in the field of high-temperature alloys is nevertheless constrained by its low room-temperature toughness, which exhibits extreme brittleness, and its somewhat inadequate strength at high temperatures [5–7]. Researchers added Mo to NiAl alloy to create a pseudo-binary eutectic structure in order to improve its characteristics. The room temperature fracture toughness of NiAl-xMo (x =7.8–16) alloy steadily increased with the increase of Mo content, and the room temperature plasticity and fracture toughness of NiAl-Mo alloy were both enhanced [8–15]. One of them, NiAl-9Mo alloy, also performs well at high temperatures [9, 10, 16].

Zr is a useful element for microalloying NiAl-Mo alloy and optimizing its microstructure and characteristics. The NiAl eutectic cells and NiAl-Mo lamellae can be improved by adding a tiny quantity of Zr, which also strengthens the material's fine grains and increases the material's strength and toughness. The high-temperature strength of NiAl-Mo alloy was also significantly improved by adding Zr, forming the Ni2AlZr phase (Heusler phase) [17–20]. However, the Heusler phase was distributed at the grain boundaries, increasing the brittle fracture tendency of the NiAl--Mo alloy [21]. Consequently, it is crucial to look at ways to enhance NiAl-Mo alloy by adding Zr without sacrificing toughness.

The characteristics of the NiAl alloy are significantly influenced by the preparation procedure. The most popular process for creating NiAl alloy is arc smelting, but because of the coarse grain size causing by the slower cooling rate, NiAl alloy has a lower fracture strength [22, 23]. The suction cast-

*Corresponding author: e-mail address: qiyihui@lnut.edu.cn
**Corresponding author: e-mail address: wangyongsll@163.com

Table 1. The composition of NiAl-9Mo-xZr alloys in the present work (at.%)

Alloy	Ni	Al	Mo	Zr
A1	45.5	45.5	9.0	0
A2	45.5	45.0	9.0	0.5
A3	45.5	44.5	9.0	1.0
A4	45.5	44.0	9.0	1.5

ing method draws high-temperature metal liquid from the molten pool into the water-cooled copper crucible through pressure differential, achieves rapid solidification or quasi-rapid solidification through quick cooling by changing the lamellar orientation or refining the lamellae, which is a novel technique for making high--temperature structural materials that has emerged in the recent year [24]. According to some studies, the plasticity and fracture strength of the suction cast NiAl-Cr(Mo) alloys significantly improved [9–15, 21, 25], showing better plasticity than with other methods.

In this paper, the NiAl-9Mo-xZr alloy prepared by the electric arc furnace melting procedure was utilized as a comparison sample to explore the effects of the Zr element's inclusion quantity on the alloy's microstructure and characteristics. XRD and SEM were used to characterize the microstructure of the material. The impact of the suction casting method and Zr element coupling on the microstructure and high-temperature characteristics of the NiAl-9Mo-xZr alloy was investigated in conjunction with hardness and high-temperature compression testing.

2. Materials and methods

In this paper, NiAl-9Mo-xZr alloys were prepared using Ni, Al, Mo, and Zr as the raw materials, all of 99.99 % purity, and adding different contents of Zr. The samples are numbered, and the corresponding composition (atomic percentage) is shown in Table 1.

All raw materials were melted in a non-consumable vacuum arc furnace under the protection of argon. The alloy was repeatedly melted and rolled over in the crucible to create button-shaped ingots, often referred to as "as-cast", in order to ensure the consistency of alloy composition. The "vacuum pumping – argon filling" method of cleaning the furnace was first used to create a vacuum in the furnace cavity that may reach 10^{-5} Pa. Argon protection is used throughout the melting process to minimize oxidation and burning loss while preparing the sample. The sponge titanium placed in the crucible was melted first before the experimental raw materials were, and as it melted, oxygen from the furnace cavity was absorbed, reducing the oxidation and burning loss of the experimental raw materials. It was believed that the alloy composition was consistent with the nominal composition since the overall mass loss of the alloy ingot during the smelting process was less than 0.5 % [9, 21]. 20 g of the A3 alloy button ingot was taken and placed in the crucible for remelting to prepare a suction-cast alloy. The molten A3 alloy was drawn into a copper mold with a diameter of 3 mm by negative pressure after it had completely melted. After the alloy was formed, the as-cast alloy was placed in a high-temperature resistance furnace for homogenization heat treatment. After two hours of treatment at 1473 K, the furnace was cooled to produce a homogeneous structure.

A quarter of the size and representative pieces were taken from the alloy ingot randomly. An Axiovert200 mat Optical Microscope and S-3000 N Scanning Electron Microscope (SEM) were used to examine the microstructure of the as-cast and suction-cast alloys. After using sandpaper to polish the metallographic sample, alcohol was used to clean it ultrasonically, then blown dry. The corrosion inhibitor is a mixture of 15 g $FeCl_3$, 15 mL HCl, and 65 mL CH_3COOH. By wiping, the corrosion time was about 10 seconds. Using a Japanese Rixue D/Max2500 X-ray diffractometer for the phases analysis of the as-cast sample, Cu target diffraction was used for the experiment (λ = 0.154157 nm), acceleration voltage of 40 kV, current of 30 mA, and the arrange of 2θ was 10°–90° .

The samples' hardness was tested using an HR--150DT Rockwell hardness tester and a Vickers hardness tester at room temperature. The sample was prepared using the same procedure as the metallographic sample. To lessen the impact of strain hardening, the control force during preparation should not be excessive. On the hardness test surface, 5 spots were randomly measured along the cross diagonal, and the average value was taken. The dimensions are cut from various alloy ingots using a wire cutter to create a 4 mm by 6 mm compression sample. All sample sections were polished with 1200 # sandpaper to provide a level surface before the test. On the Gleeble-1500 thermal simulation experimental machine, the compression test was performed. The experimental temperatures were 1173 and 1273 K, with a ± 2 K precision in temperature control with a thermocouple welded to the sample's surface. Under a heating rate of 10 K s^{-1}, the samples were crushed and then naturally cooled. Four compression pieces were tried for each sample to lower the error, and the strain rate used was 2.78×10^{-3} s^{-1}.

3. Results and discussion

The microstructural morphology and phase compositions were characterized by SEM. Figure 1 depicts

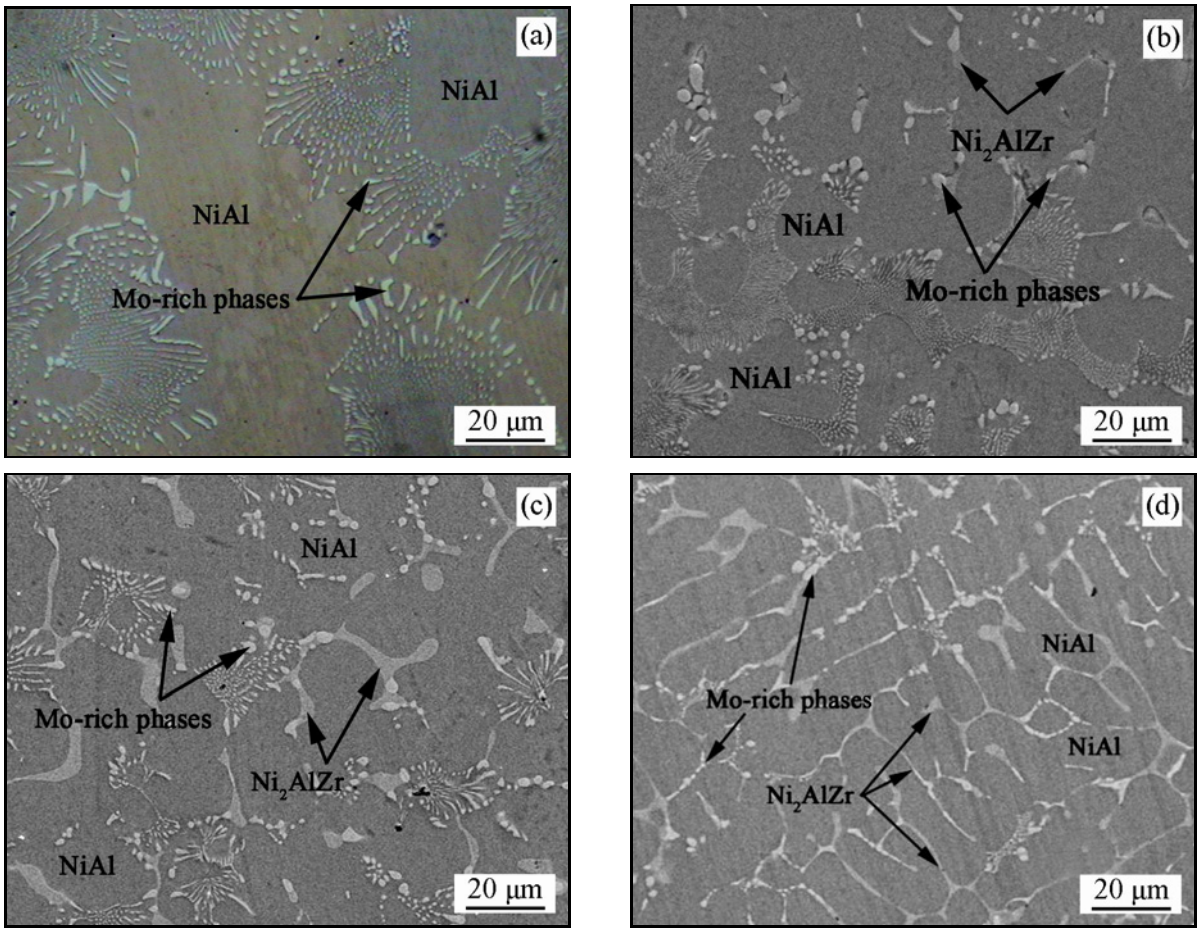

Fig. 1. Microstructures of the as-cast NiAl-9Mo-xZr alloy with various Zr contents.

the typical microstructure of the as-cast alloy following etching. The microstructure can be characterized by coarse NiAl matrix grains almost surrounded by the luminous white Mo phases, and the left ones are inlaid within the cell or at the middle of the unit cell composed of tiny particles because of the coherent relationship, which was mentioned in previous work [26]. Each phase's volume fraction in the eutectic fulfils the given Eq. (1):

$$\frac{V_{\alpha-\mathrm{Mo}}}{V_{\beta-\mathrm{NiAl}}+V_{\alpha-\mathrm{Mo}}} > \frac{1}{\pi}. \tag{1}$$

Eutectic alloys commonly generate either a rod-like structure or a sheet-like structure. Since the lamellar spacing in the unit cells is smaller than that of the cell boundaries, as can be observed from Fig. 1a, the rod-shaped Mo phases expand radially perpendicular to the NiAl cell boundaries. According to anterior studies [26, 27], it seemed that mechanical rearrangement proceeded at the cell boundary. The core of the unit cell generated spherical Mo phases throughout the preparation procedure, which was reported earlier. The eutectic cell size of the NiAl-9Mo alloy considerably shrinks with the addition of Zr, and near the cell

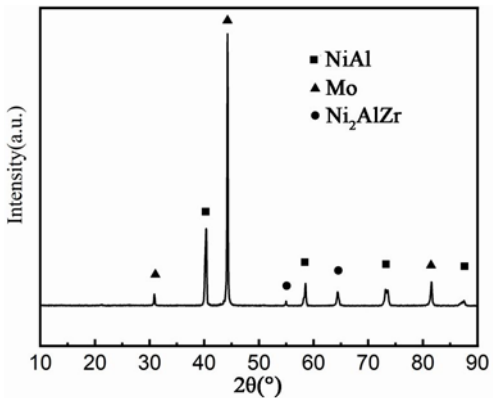

Fig. 2. X-ray diffraction patterns of the as-cast A4 alloy.

boundary, discontinuous and semi-continuous mesh-like phases are produced [9]. The sizes of the eutectic cell continue to shrink as the Zr content increases.

The calibration of the diffraction peaks reveals that the discontinuous phase at the cell border is most likely the Heusler phase, connected to the alloy's uneven eutectic cell structure. The B2-ordered body center structures give way to the L21 structures during

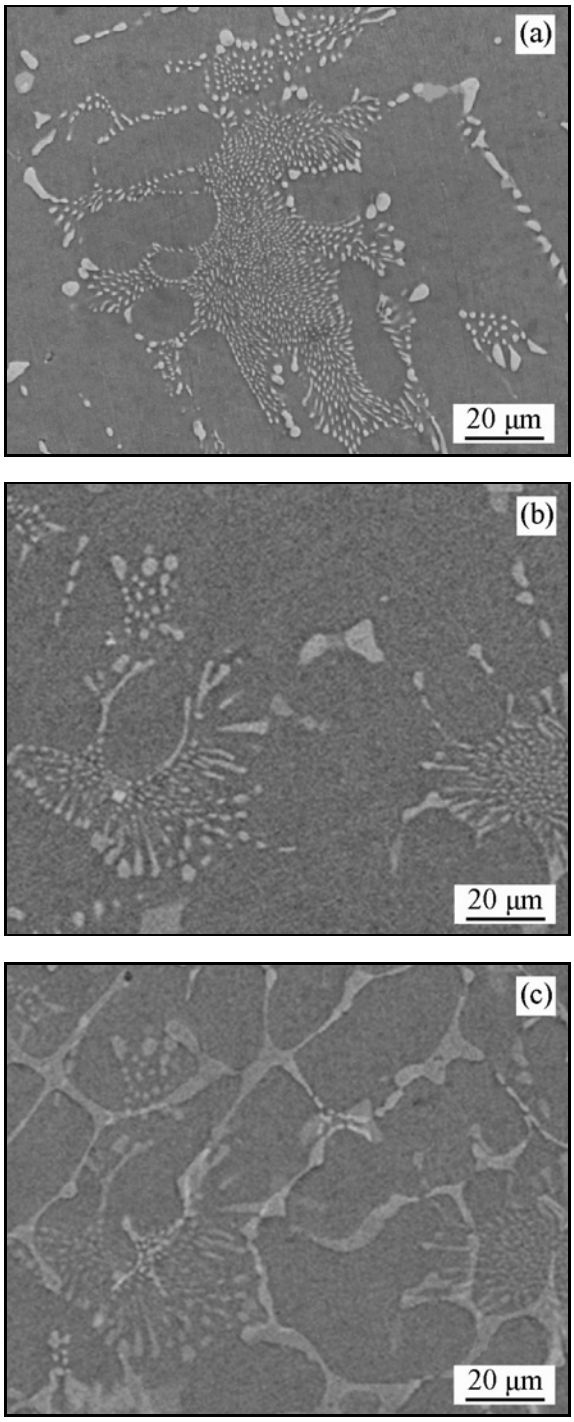

Fig. 3. Microstructures of the NiAl-Mo-xZr alloy after heat treatment (a) A2, (b) A3, and (c) A4.

the Heusler phase. The Heusler phase is more ordered than NiAl in terms of ordering [28]. NiAl-Mo alloy has a melting point (1718 K) greater than the Heusler phase (1623 K). First, the NiAl phases formed during solidification, and then, at the cell boundaries, the semi-continuous Heusler phases formed due to a eutectic reaction.

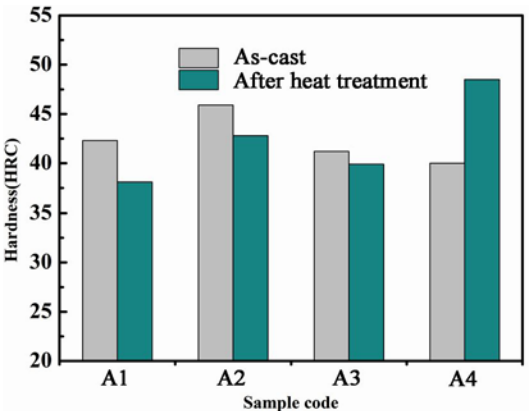

Fig. 4. Hardness of the NiAl-Mo-xZr alloy.

Figure 3 is the microstructure of the NiAl-Mo-xZr alloy after homogenization heat treatment at 1473 K for 2 h. It can be seen from Fig. 3 that the morphology of NiAl-9Mo-xZr eutectic cells in the structure remains unchanged after heat treatment but has grown significantly. The Mo phases become more coarse, and their distribution is scattered. The Heusler phases of the A2 alloy essentially vanish in Fig. 3a. This is because the Heusler phase transforms into the Zr-rich phase following homogenization, and the Mo element is most likely to take part in the Heusler phase's phase transition process [29]. Mo atoms diffuse to Heusler phases at high temperatures, lowering their order and stability until the Heusler phases transform into the Zr-rich NiAl phases with great stability.

The NiAl-Mo-xZr alloy's Rockwell hardness as-cast and after homogenization heat treatment are compared in Fig. 4. As demonstrated in Fig. 2, the 0.5 % Zr addition refines the NiAl-9Mo alloy's coarse eutectic cell structure. Comparing the hardness of various NiAl-9Mo-xZr alloys, the as-cast A2 alloy has the maximum hardness because of the synergistic impact of the solid solution strengthening of Zr atoms and the second-phase strengthening of Heusler phases on the precipitation strengthening action of Mo particles on dislocation pinning [28–30]. Mo phases in the NiAl eutectic cells dissolve more readily as Zr concentration increases, which reduces the Mo phase's ability to enhance precipitation. The hardness of A3 and A4 alloys is reduced due to the limited second phase strengthening impact of the Heusler phase at the cell boundaries. The amount of Zr has a weak effect on the hardness of as-cast NiAl-9Mo-xZr. The size of the eutectic cells grows coarser, the Heusler phases shrink, and the associated second phases strengthening lessen after homogenization heat treatment at 1473 K. The strengthening effect of the second phase of the A4 alloy is weakened after heat treatment due to a decrease in the Heusler phases content, but its hardness is greatly increased as a result of the solid solution strengthening

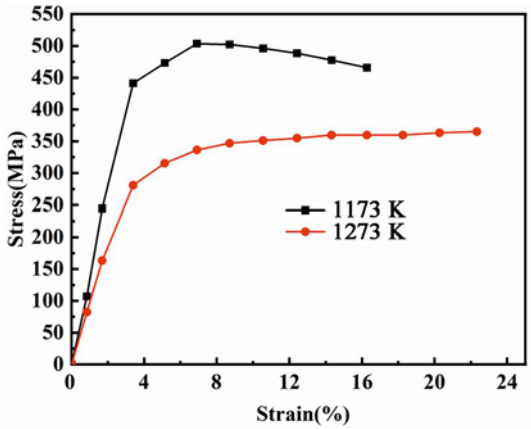

Fig. 5. The stress-strain curves of the as-cast A3 alloy.

impact of Zr dissolved in the NiAl matrix.

As the addition of Zr reaches 1 %, it causes the formation of continuous Heusler phases at the eutectic cells boundaries of the NiAl-9Mo-xZr alloy, which significantly reduces the alloy's compressive plasticity, causes cracks to spread quickly in the eutectic cells boundaries area at the early stage of compression deformation, and further deteriorates the alloy's compressive plasticity [9]. The compression stress-strain curves of the A3 alloy at 1173 and 1273 K are shown in Fig. 5. The A3 alloy's compressive yield strength is 450 MPa (1173 K) and 275 MPa (1273 K). As temperature rises, the compressive yield strength declines. The work hardening of the sample is most noticeable at the beginning of deformation. As the stress reaches its maximum value, the stress steadily reduces as the strain increases. The sample looses strength as the temperature rises, and it takes less time to achieve the stress peak at 1273 K than at 1173 K because higher temperatures enhance the metal atoms' propensity to diffuse, decrease the barrier to dislocation movement, and weaken alloys. High temperatures cause the elastic modulus, the Perner force of dislocation movement, the degree of grains coordination during deformation, the alloy's plasticity, and its strength to drop.

In Fig. 6, the microstructure of the suction-cast A3 alloy is depicted and contrasted with that of the as--cast A3 alloy (Fig. 1). Besides the great refinement of the Mo phase, the significant difference from the as--cast alloy is that the Mo phases at the cell borders expand perpendicularly and are coarser than Mo phases within the cell. Heusler phases eutectic microstructure forms along the NiAl phase boundary, which can be found in similar structures in the preliminary research [32]. Various magnifications of the observation of the microstructure illustrated in Figs. 6a,b show that the microstructure of the suction-cast alloy is finer as a result of the rapid cooling. Suction-cast A3 alloy eutectic lamella thickness is roughly 3 and 20 μm in size.

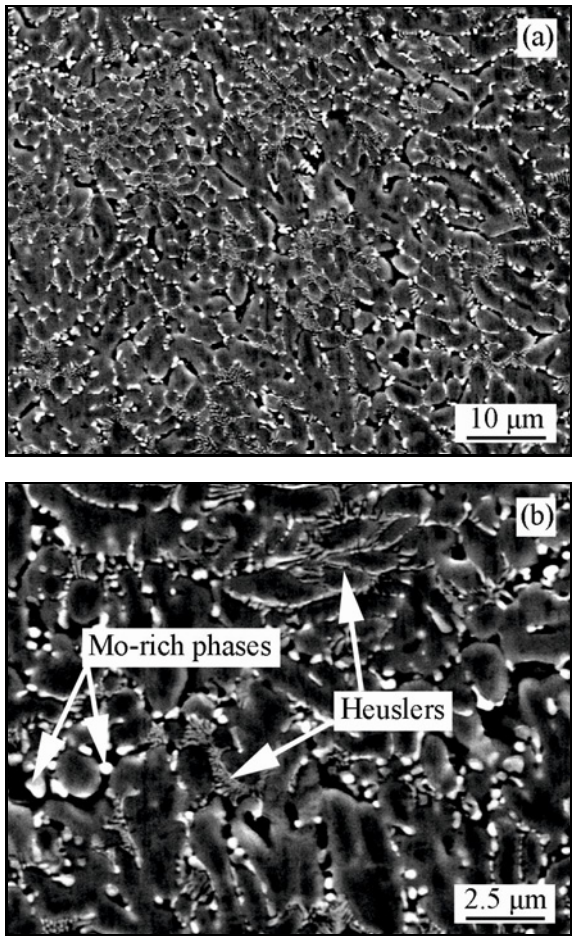

Fig. 6. Microstructures of the A3 alloy: (a) as-cast and (b) suction-cast.

It demonstrates the NiAl-9Mo-xZr alloy's eutectic cell size may be drastically reduced during the suction casting process [10, 24, 33].

According to Vickers hardness measurements, the suction-cast A3 alloy has a harder surface than the as-cast A3 alloy, with microhardness values of 396 HV and 630 HV, respectively. The microstructure of suction-cast alloy is well refined [11], with narrow eutectic cell sizes [10, 12, 15], which retains a more even distribution of the Heusler phase formed at the cell boundary, and fine grain strengthening and the second phase strengthening that cooperate in conjunction to improve the alloy's hardness.

The results of a high-temperature compression test on A3 alloys that were as-cast and suction-cast are shown in Fig. 7. As the suction-cast A3 alloy reaches the yield at 1273 K, a transient steady state will occur and then strain softening will happen. But there is no softening of the as-cast state. This is required for the alloy to develop a precisely tailored structure during the suction casting process. Recrystallization, which enhances plasticity and strain soften-

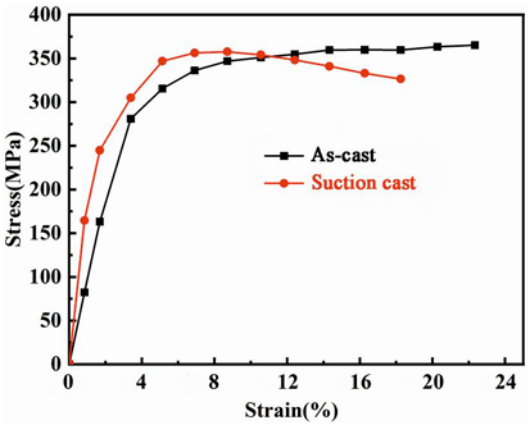

Fig. 7. The compressive stress-strain curves of the suction-cast A3 alloy at 1273 K.

ing, happens in a section of the eutectic cells that are now in a metastable state when high temperature and compressive stress are combined during compression. At 1273 K, the compressive yield strength of A3 alloy prepared by the suction-cast method reaches 350 MPa, enlightening that the samples produced this way may guarantee and achieve superior high-temperature strength.

4. Conclusions

In the present work, the as-cast NiAl-Mo-xZr alloy features a typical eutectic cell microstructure, with white-layered Mo phases and discontinuous Heusler phases making up the cell boundaries. Heusler phases content increased with the increasing Zr contents. The eutectic cell structure of the NiAl-Mo-xZr alloy becomes rougher after homogenization heat treatment. The Mo phases dissolve in the NiAl cells, which has an impact on the strengthening of the precipitation. The eutectic cells of the NiAl-9Mo-1Zr alloy made by suction casting technique are greatly refined, and the average eutectic lamella thickness is around 3 μm. The discontinuous Heusler phases disappeared partially or entirely. The suction-cast NiAl-9Mo-1Zr alloy has a higher high-temperature compressive strength than the as-cast alloy due to the fine grain strengthening and the second phase strengthening of the Heusler phases, which exceeds 350 MPa at 1273 K.

Acknowledgement

This research was supported by the Youth Science Fund and Research Startup Fund of Northeast Petroleum University(2020QNL-09).

References

[1] X. Chen, Y. Liu, L. Zhang, S. Wang, X. Qu, Phase formation and evolution during transient liquid phase sintering of MIM418 superalloy with master alloy addition, Journal of Alloys and Compounds 829 (2020) 154583. https://doi.org/10.1016/j.jallcom.2020.154583

[2] M. Zagula-Yavorska, Oxidation behavior of non-modified and rhodium- or palladium-modified aluminide coatings deposited on CMSX-4 superalloy, Metals 8 (2018) 613. https://doi.org/10.3390/met8080613

[3] R. Qin, H. D. Fu, Y. W. Kang, X. Z. Zhou, Z. H. Zhang, J. X. Xie, Simulation of temperature field in directional solidification casting of Nb-Si based alloys, Chinese Journal of Engineering 42 (2020) 1165–1173. https://doi.org/10.13374/j.issn2095-9389.2019.10.02.001

[4] M. D. Gan, X. Y. Zhong, J. Feng, Research status and prospects of aerospace high-temperature structural materials, Journal of Kunming University of Science and Technology (Natural Sciences) 46 (2021) 24–26. https://doi.org/10.16112/j.cnki.53-1223/n.2021.06.422

[5] K. L. Cao, W. Yang, J. Zhang, C. Liu, P. Qu, H. Su, J. Zhu, L. Liu, Solidification characteristics and as-cast microstructures of a Ru-containing nickel-based single crystal superalloy, Journal of Materials Research and Technology 11 (2021) 474–486. https://doi.org/10.1016/j.jmrt.2021.01.043

[6] Z. Liu, H. W. Ning, Z. Q. Lin, D. Wang, Influence of spark plasma sintering parameters on the microstructure and room-temperature mechanical properties of NiAl-28Cr-5.5Mo-0.5Zr alloy, Acta Metallurgica Sinica 57 (2021) 1579–1587. https://doi.org/10.11900/0412.1961.2020.00346

[7] N. T. H. Trung, H. S. M. Phuong, M. Starostenkov, Molecular dynamics simulation of displacement cascades in B2 NiAl, Letters on Materials 9 (2019) 168–172. https://doi.org/10.22226/2410-3535-2019-2-168-172

[8] J. J. Gao, Z. L. Zhao, L. F. Wei, K. Cui, L. Liu, Microstructure and microhardness of directionally solidified NiAl-W eutectic alloy, Rare Metals 39 (2020) 1174–1180. https://doi.org/10.1007/s12598-019-01268-5

[9] H. Ning, D. Wang, B. Wang, G. Liu, Investigations on the NiAl-Cr(Mo) eutectic alloy with optimized microstructure and improved room-temperature compressive properties, Materials Science and Engineering A 813 (2021) 141138. https://doi.org/10.1016/j.msea.2021.141138

[10] A. A. Zaitsev, Zh. A. Sentyurina, E. A. Levashov, Yu. S. Pogozhev, V. N. Sanin, D. A. Sidorenko, Structure and properties of NiAl-Cr(Co,Hf) alloys prepared by centrifugal SHS casting followed by vacuum induction remelting, Part 2 – Evolution of the structure and mechanical behavior at high temperature, Materials Science & Engineering A 690 (2017) 473–481. https://doi.org/10.1016/j.msea.2017.02.089

[11] C. Gombola, A. Kauffmann, G. Geramifard, M. Blankenburg, M. Heilmaier, Microstructural investigations of novel high temperature alloys based on NiAl-

-(Cr,Mo), Metals 10 (2020) 961. https://doi.org/10.3390/met10070961
[12] J. Peng, P. Franke, H. J. Seifert, Experimental investigation and CALPHAD assessment of the eutectic trough in the system NiAl-Cr-Mo, Journal of Phase Equilibria & Diffusion 37 (2016) 592-600. https://doi.org/10.1007/s11669-016-0490-y
[13] L. Sheng, Y. Yang, T. Xi, Effect of heat treatment on morphology evolution of Ti_2Ni phase in Ti-Ni-Al--Zr alloy, IOP Conference Series Materials Science and Engineering 322 (2018) 022040. https://doi.org/10.1088/1757-899X/322/2/022040
[14] L. Y. Sheng, B. N. Du, J. T. Guo, Microstructure and mechanical properties of zirconium doped NiAl/Cr(Mo) hypoeutectic alloy prepared by injection casting, IOP Conference 167 (2017) 012052. https://doi.org/10.1088/1757-899X/167/1/012052
[15] V. V. Sanin, Y. Y. Kaplansky, M. I. Aheiev, E. A. Levashov, M. I. Petrzhik, M. Ya. Bychkova, A. V. Samokhin, A. A. Fadeev, V. N. Sanin, Structure and properties of heat-resistant alloys NiAl-Cr-Co-X (X = La, Mo, Zr, Ta, Re) and fabrication of powders for additive manufacturing, Materials 14 (2021) 3144. https://doi.org/10.3390/ma14123144
[16] J. F. Zhang, J. Shen, Z. Shang, Z. R. Feng, L. Wang, H. Fu, Regular rod-like eutectic spacing selection during directional solidified Ni-Al-9Mo eutectic in situ composite, Journal of Crystal Growth 329 (2011) 77–81. https://doi.org/10.1016/j.jcrysgro.2011.06.049
[17] J. Albiez, H. Erdle, D. Weygand, T. Böhlke, A gradient plasticity creep model accounting for slip transfer/activation at interfaces evaluated for the intermetallic NiAl-9Mo, International Journal of Plasticity 113 (2019) 291–311. https://doi.org/10.1016/j.ijplas.2018.10.006
[18] J. B. Guo, H. Zhong, Z. P. Liu, L. Yang, S. Li, Influence of fiber size and interface morphology on the electrochemical corrosion resistance of directionally solidified NiAl-9Mo eutectic alloy, Rare Metal Materials and Engineering 48 (2019) 1116–1123. https://doi.org/CNKI:SUN:COSE.0.2019-04-013
[19] J. F. Zhang, J. Shen, Z. Shang, Z.-R. Feng, L.-S. Wang, H.-Z. Fu, Microstructure and room temperature fracture toughness of directionally solidified NiAl-Mo eutectic in situ composites, Intermetallics 21 (2012) 18–25. https://doi.org/10.1016/j.intermet.2011.10.002
[20] S. Arias, L. V Sousa, C. B. M. Barbosa, A. O. S. Silva, R. Fréty, J. G. A. Pacheco, Preparation of NiAlZr-terephthalate LDHs with high Al and Zr content and their mixed oxides for cyclohexane dehydrogenation, Applied Clay Science 166 (2018) 137–145. https://doi.org/10.1016/j.clay.2018.09.020
[21] X. Han, F. Ding, Y. Qin, D. Wu, H. Xing, Y. Shi, K. Song, C. Cao, Compositional dependence of crystallization kinetics in Zr-Ni-Al metallic glasses, Vacuum 151 (2018) 30–38. https://doi.org/10.1016/j.vacuum.2018.02.001
[22] D. Wang, Y. Liang, H. Ning, B. Wang, Effects of Zr and Co on the microstructure and mechanical properties of NiAl-based alloys, Journal of Alloys and Compounds: An Interdisciplinary Journal of Materials Science and Solid-state Chemistry and Physics 883 (2021) 160815. https://doi.org/10.1016/j.jallcom.2021.160815
[23] L. Y. Sheng, J. T. Guo, C. Lai, Effect of Zr addition on microstructure and mechanical properties of NiAl/Cr(Mo) base eutectic alloy, Acta Metallurgica Sinica – Chinese Edition 51 (2015) 828–834.
[24] S. Talaş, G. Oruç, Characterization of TiC And TiB_2 reinforced nickel aluminide (NiAl) based metal matrix composites cast by in situ vacuum suction arc melting, Vacuum 172 (2019) 109066. https://doi.org/10.1016/j.vacuum.2019.109066
[25] L. Li, L. Wang, L. Zhao, X. Wang, Microstructure and adhesion strength of NiAl coating prepared on Q235 substrate by combustion synthesis assisted with Cu-Zn interlayer, Surface & Coatings Technology 344 (2018) 564–571. https://doi.org/10.1016/j.surfcoat.2018.03.076
[26] A. Thoemmes, I. A. Bataev, D. V. Lazurenko, A. A. Ruktuev, I. V. Ivanov, C. R. M. Afonso, A. Stark, A. M. Jorge Jr., Microstructure and lattice parameters of suction-cast Ti-Nb alloys in a wide range of Nb concentrations, Materials Science and Engineering A 818 (2021) 141378. https://doi.org/10.1016/j.msea.2021.141378
[27] L. M. Sang, Y. Xu, P. Fang, H. Zhang, Y. Ciu, X. Liu, The influence of cooling rate on the microstructure and phase fraction of gas atomized NiAl3 alloy powders during rapid solidification, Vacuum 157 (2018) 354–360. https://doi.org/10.1016/j.vacuum.2018.08.057
[28] D. Wang, Y. Liang, H. Ning, B. Wang, Effects of Zr and Co on the microstructure and mechanical properties of NiAl-based alloys, Journal of Alloys and Compounds 883 (2021) 160815. https://doi.org/10.1016/j.jallcom.2021.160815
[29] G. Geramifard, C. Gombola, P. Franke, H. J. Seifert, Oxidation behaviour of NiAl intermetallics with embedded Cr and Mo, Corrosion Science 177 (2020) 108956. https://doi.org/10.1016/j.corsci.2020.108956
[30] Y. Y. Kaplanskii, A. V. Korotitskiy, E. A. Levashov, P. A. Loginov, A.V. Samokhin, I. A. Logachev, Microstructure and thermomechanical behavior of Heusler phase Ni_2AlHf- strengthened NiAl-Cr(Co) alloy produced by HIP of plasma-spheroidized powder, Materials Science and Engineering A 729 (2018) 398–410. https://doi.org/10.1016/j.msea.2018.05.087
[31] K. Bochenek, M. Basista, Advances in processing of NiAl intermetallic alloys and composites for high temperature aerospace applications, Progress in Aerospace Sciences 79 (2015) 136–146. https://doi.org/10.1016/j.paerosci.2015.09.003
[32] L. Y. Sheng, W. Zhang, J. T. Guo, Microstructure evolution and elevated temperature compressive properties of a rapidly solidified NiAl-Cr(Nb)/Dy alloy, Materials & Design 30 (2009) 2752–2755. https://doi.org/10.1016/j.matdes.2008.10.022
[33] W. Lei, J. Shen, Effect of heat treatment on the microstructure and elevated temperature tensile property of Fe-doped NiAl-Cr(Mo)-(Hf,Dy) eutectic alloy, Materials Science and Engineering 654 (2016) 177–183. https://doi.org/10.1016/j.msea.2015.12.043